Int. J. Heat Mass Transfer. Vol. 35, No. 5, pp. 1293–1306, 1992
Printed in Great Britain

0017–9310/92 $5.00 + 0.00

Transient natural convection over a heat generating vertical cylinder

K. VELUSAMY
Thermal Hydraulics Section, Indira Gandhi Centre for Atomic Research, Kalpakkam 603102, India

and

VIJAY K. GARG†
Department of Mechanical Engineering, University of Pittsburgh, Pittsburgh, PA 15261, U.S.A.

(*Received* 22 *January* 1990 *and in final form* 24 *April* 1991)

Abstract—A numerical solution for the transient natural convection over heat generating vertical cylinders of various thermal capacities and radii is presented. A fully implicit finite difference technique is used to solve the non-linear set of equations. The rate of propagation of the leading edge effect is given special consideration. It is found that this rate, predicted by the one-dimensional conduction solution, is slower than that resulting from the boundary layer solution. Also, it increases as the radius and thermal capacity of the cylinder decrease, and as the surface heat flux increases. The transient boundary layer thickness is found to exceed its steady-state value while the transient average heat transfer coefficient is found to reach a minimum, as low as 53% of its steady-state value for the highest value of the modified Grashof number studied. Excellent agreement with previous experimental steady-state data as well as with one-dimensional theoretical results is obtained.

1. INTRODUCTION

IN THE event of pump or power failure, the heat energy from the nuclear reactor is removed solely by natural convection. Following sudden stoppage of the pump, it takes some time for the natural convection to set in. During this period, heat is transferred mainly by conduction, and it is known that the heat transfer coefficient passes through a minimum before reaching the final steady-state value. The history of the transient heat transfer coefficient and the time required for the natural convection flow to set in are essential for reactor calculations.

Illingworth [1] initiated such a transient analysis for an infinite flat plate brought suddenly to an isothermal temperature different from the surrounding, otherwise quiescent, fluid. He presented the velocity and temperature solutions for a Prandtl number of unity. For such a case, no leading edge effect prevails and heat is transferred purely by one-dimensional conduction. However, for real geometries of finite length, a leading edge effect does exist and the transient one-dimensional analysis is valid, for any axial location, only until the leading edge effect reaches that location. This effect is marked by the entrainment of ambient fluid and only boundary layer solutions are valid thereafter. Schetz and Eichhorn [2], and Menold and Yang [3] studied such one-dimensional transients for time-varying surface temperatures and heat flux boundary conditions over a flat plate. These analyses, however, do not give the duration of the one-dimensional process that collapses upon the arrival of the leading edge effect.

Siegel [4] used the Karman–Pohlhausen integral method to solve the momentum and energy boundary layer equations for a semi-infinite flat plate. He analyzed the problem for a step change both in surface temperature and in heat flux, and is the first to point out the effect of leading edge and time duration of the one-dimensional conduction process. Subsequently, Goldstein and Eckert [5] reported experimental results for a flat plate supplied with sudden heat input, and verified the predictions of Siegel [4]. Gebhart [6] analyzed the case of a semi-infinite flat plate with thermal capacity using the integral technique, and obtained results in close agreement with the experimental data of Gebhart and Adams [7]. Goldstein and Briggs [8] presented solutions for predicting the duration of the one-dimensional process from the results of an infinite plate. Their analysis includes various boundary conditions such as a step change in surface temperature, surface heat flux, plates of various thermal capacity and fluids of various Prandtl numbers.

Mollendorf and Gebhart [9], and Mahajan and Gebhart [10] observed the leading edge effect propagation and found that this effect reaches any axial position about 20% faster than that predicted by Goldstein and Briggs [8]. Yang [11] and Nanbu [12]

† Present address: NASA Lewis Research Center, Cleveland, OH 44135, U.S.A.

NOMENCLATURE

a, b	arbitrary constants
Bi	Biot modulus
c	thermal capacity of the cylinder per unit surface area
e	small number for determining the arrival of the leading edge effect
g	acceleration due to gravity
Gr_x	modified local Grashof number, $(g\beta q'' x^4/kv^2)$
Gr_L	modified Grashof number at $x = x_{end}$
h	local heat transfer coefficient
k	thermal conductivity of the fluid
k_m	thermal conductivity of the cylinder material
L.E.E.	leading edge effect
m	iteration index
Nu_x	local Nusselt number, hx/k
Pr	Prandtl number of the fluid
q''	instantaneous energy generation rate within the cylinder per unit surface area
q'''	volumetric energy generation rate
q_N	normalized local heat flux, $-(k/q'')(\partial t/\partial r)\|_{r=r_0}$
Q	thermal capacity parameter
r	radial coordinate measured from the centerline of the cylinder
r_0	radius of the cylinder
R	dimensionless radial coordinate
R_0	fourth root of the modified Grashof number with r_0 as length
R_b	edge of the boundary layer
ΔR	grid size in the radial direction
t	temperature of the fluid within the boundary layer
T	dimensionless temperature
u, v	velocity components in the x-, r-directions, respectively
U, V	dimensionless velocity components in the X-, R-directions, respectively
x	axial coordinate measured upward
X	dimensionless axial coordinate
X_{BL}	penetration distance of the leading edge effect based on the present boundary layer solution
X_{BR}	penetration distance of the leading edge effect based on the Brown and Riley criterion
X_{GB}	penetration distance of the leading edge effect based on the Goldstein and Briggs criterion
X_J	penetration distance of the leading edge effect based on Joshi's criterion of no overshoot in the mass flow rate
ΔX	grid size in the axial direction.

Greek symbols

α	thermal diffusivity of the fluid
β	coefficient of volumetric expansion of the fluid
ε	small number for test of convergence
η	pseudo-similarity variable, $((r^2-r_0^2)/2r_0)\{g\beta(t_s-t_\infty)/4xv^2\}^{1/4}$
η_w	$R_0(5X)^{1/5}$
ν	kinematic viscosity of the fluid
ξ	stretched axial coordinate, $2\{4xv^2/g\beta(t_s-t_\infty)r_0^4\}^{1/4}$
τ	dimensionless time
$\hat{\tau}$	time
$\Delta\tau$	step size in time
ψ	dummy variable.

Subscripts and superscript

c	value at the centerline of the cylinder
s	value at the cylinder surface
ss	value at steady state
∞	value in the free-stream
end	value at downstream end
$\bar{}$	average value from $x = 0$ to x_{end}.

analyzed the transient boundary layer equations and concluded that the departure from the one-dimensional process occurs at a critical time when an essential singularity in the governing equations appears. Brown and Riley [13] pointed out that this critical time resulted in a leading edge propagation criterion different from that proposed by Goldstein and Briggs [8]. Recently Joshi [14] compared four different propagation criteria with the experimental results of Mollendorf and Gebhart [9], and Mahajan and Gebhart [10]. He concluded that the propagation distance based on the criterion of 'no overshoot in the mass flow rate during the one-dimensional process' yields the fastest propagation amongst all the four criteria. This was found to be in close agreement with the experiments in water.

Hellums and Churchill [15] solved the unsteady boundary layer equations using a finite difference method for a semi-infinite isothermal flat plate in air, while Sammakia *et al.* [16] analyzed the case of a flat plate with constant heat flux and finite heat capacity. The latter included the effect of radiation in their analysis and compared their numerical results with the experimental data in air. They concluded that the effect of radiation is negligible at high heat flux levels. Later, Sammakia *et al.* [17] presented numerical and experimental results of natural convection adjacent to a vertical plate of finite heat capacity in water. Carey

[18, 19] analyzed the flat plate in high Prandtl number fluid with zero and finite thermal capacity, and confirmed the existence of a dual layer structure during the entire transient process. He also found that the time to reach steady state was proportional to Prandtl number raised to the power 3/5.

Joshi and Gebhart [20] analyzed the one-dimensional transient process adjacent to a flat plate of finite thermal capacity subjected to sudden changes in heat flux and temperature in water at its density extremum. More recently Joshi and Gebhart [21] studied analytically and experimentally the case of a flat plate subjected to a sudden change of heating rate. During this process of switching over from one initial steady state to another, periodic disturbances were observed to propagate downstream from the leading edge. These disturbances lead to transient transition to turbulence before relaminarization takes place, and this transition increases the heat transfer effectiveness. Gokhle [22] analyzed the case of transient natural convection adjacent to an isothermal flat plate, with heat sources in air and water, by the finite difference method. The heat source was taken to be a function of the local temperature gradient.

While the flat plate has been studied in detail, the cylinder, which is the geometry for heat generating fuel rods in a reactor, has been given little attention. It is well known that the boundary layer over a slender cylinder is thicker than that over a flat plate. Hence the results of flat plate analysis do not apply directly to slender cylinders and they deserve a separate study. Goldstein and Briggs [8] carried out a one-dimensional study of transient natural convection from cylinders. They presented analytical solutions for the duration of the one-dimensional process from the conduction analysis for infinite cylinders. Subsequently, Dring and Gebhart [23] presented experimental results for the transient average temperature of Nichrome wires in silicone oils and in air. They also compared their experimental results with the pure conduction results, and with a simplified quasistatic theory that yields a simple exponential solution for the temperature response. The quasistatic theory failed, however, for silicone fluids. Even for air, the conduction solution was found to be better than that predicted by this theory.

Some steady-state analyses for a cylinder also exist. Amongst them, Minkowycz and Sparrow [24] obtained the steady boundary layer velocity and temperature profiles for isothermal cylinders of various radii placed in air using the local non-similarity method. Nagendra *et al.* [25] carried out a numerical study of steady boundary layer equations for cylinders subjected to uniform heat flux and compared their predictions with the experimental results of their earlier study in water. They found that the difference of heat transfer coefficients between the cases of isothermal and constant heat flux cylinders is about 6%. Chen and Yuh [26] studied steady heat and mass transfer processes near cylinders with uniform wall heat and mass fluxes, and wall temperature numerically. Their study covered a wide range of radii and Prandtl numbers. Subsequently Chen [27] studied the power law variation of wall heat flux for cylinders in steady natural convection flow for various Prandtl numbers. More recently Lee *et al.* [28] solved the steady boundary layer equations using the non-similar transformation followed by the finite difference method with the spline interpolation technique. They considered the wall temperature varying as a function of the axial coordinate.

Herein we present a numerical solution of the transient natural convection adjacent to heat generating, vertical cylindrical fuel rods of various thermal capacities, radii and surface heat flux. We compare the boundary layer solution with the one-dimensional conduction solution, and compute the leading edge propagation time as proposed by Brown and Riley [13], and by Joshi [14]. The accuracy of the numerical calculations is assessed by comparison with the steady-state local non-similar results of Minkowycz and Sparrow [24], the experimental and analytical results of Nagendra *et al.* [25], and the one-dimensional results of Goldstein and Briggs [8] obtained through Laplace transforms.

2. ANALYSIS

The transient natural convection boundary layer equations adjacent to a heat generating, vertical cylinder (see inset of Fig. 10) for laminar, constant property, viscous flow with Boussinesq approximation are

$$\frac{\partial(RU)}{\partial X}+\frac{\partial(RV)}{\partial R}=0 \tag{1}$$

$$\frac{\partial U}{\partial \tau}+U\frac{\partial U}{\partial X}+V\frac{\partial U}{\partial R}=T+\frac{1}{R}\frac{\partial}{\partial R}\left(R\frac{\partial U}{\partial R}\right) \tag{2}$$

$$\frac{\partial T}{\partial \tau}+U\frac{\partial T}{\partial X}+V\frac{\partial T}{\partial R}=\frac{1}{Pr}\frac{1}{R}\frac{\partial}{\partial R}\left(R\frac{\partial T}{\partial R}\right) \tag{3}$$

subject to the following boundary and initial conditions:

$$U=0=V=T \quad \text{at} \quad \tau=0 \text{ for all } X \text{ and } R$$

$$U=0=V \quad \text{at} \quad R=R_0 \text{ for all } X \text{ and } \tau$$

$$U=0=T \quad \text{at} \quad X=0 \text{ for all } R \text{ and } \tau$$

$$U\to 0, T\to 0 \quad \text{as} \quad R\to\infty \text{ for all } X \text{ and } \tau$$

$$Q\frac{\partial T_s}{\partial \tau}-\left.\frac{\partial T}{\partial R}\right|_{R=R_0}=1 \quad \text{for all } X \text{ and } \tau \tag{4}$$

where

$$X=\frac{x}{r_0}R_0, \quad R=\frac{r}{r_0}R_0, \quad \tau=\frac{\hat{\tau}v}{r_0^2}R_0^2$$

$$U=\frac{ur_0}{vR_0}, \quad V=\frac{vr_0}{vR_0}, \quad T=\frac{k(t-t_\infty)}{q''r_0}R_0$$

$$Q = \frac{cv}{kr_0} R_0, \quad Pr = \frac{v}{\alpha}, \quad T_s = \frac{k(t_s - t_\infty)}{q''' r_0} R_0$$

$$R_0 = \frac{r_0}{(kv^2/g\beta q''')^{1/4}},$$

fourth root of the modified Grashof number.

The boundary conditions in equation (4) imply that the temperature of the cylinder has been lumped in the radial direction. For conduction through a solid cylinder of radius r_0, internal energy generation rate q''', thermal conductivity k_m, and heat transfer coefficient h, it is easy to show that

$$\frac{(t_c - t_s)}{(t_s - t_\infty)} = \frac{hr_0}{2k_m} = Bi.$$

For air as the fluid and Cr–Ni steel as the cylinder material, the value of Bi is found to be 1.3×10^{-3} for $R_0 = 4$ at $X = 100$. For smaller values of R_0 such as 0.5, Bi is as low as 4×10^{-4}, thus justifying our assumption about the radially invariant temperature of the cylinder.

Though the temperature of the cylinder varies in the axial direction, the axial heat conduction has been neglected. The steady-state surface temperature of the cylinder has been found to vary as $T_s = bX^a$, where the constants a and b vary with R_0. The axial heat flux at any location X can be shown to be

$$k_m \frac{dt_s}{dx} = -abq'' \left(\frac{k_m}{k}\right) X^{a-1}$$

and the radial heat flux in the fluid surrounding the cylinder is

$$h(t_s - t_\infty) = \frac{bh}{R_0} \left(\frac{q''' r_0}{k}\right) X^a.$$

The ratio of the total axial heat transfer to the radial heat transfer can be shown to be $-(r_0/L)(R_0/4)(a/X)/Bi$. For $R_0 = 4$ and at $X = 100$, this ratio is found to be about -0.05. For smaller values of R_0 such as 0.5, this ratio is as small as -1.4×10^{-3}. Thus axial conduction is negligible. Also, the effect of surface radiation can be neglected for a highly polished surface.

The one-dimensional conduction forms of equations (2) and (3) are

$$\frac{\partial U}{\partial \tau} = T + \frac{1}{R} \frac{\partial}{\partial R} \left(R \frac{\partial U}{\partial R}\right) \tag{5}$$

$$\frac{\partial T}{\partial \tau} = \frac{1}{Pr} \frac{1}{R} \frac{\partial}{\partial R} \left(R \frac{\partial T}{\partial R}\right) \tag{6}$$

subject to the same initial and boundary conditions (in the radial direction) as in equations (4) for U and T. The penetration distance of the leading edge effect at any instant τ as proposed by Brown and Riley [13] is

$$X_{BR}(\tau) = \int_0^\tau \max\,[U(\psi, R)]\, d\psi \tag{7}$$

where the velocity $U(\tau, R)$ is calculated from the solution of equations (5) and (6). The actual penetration distance from the present boundary layer solution, estimated by the appearance of the cross stream velocity component, that is, by

$$V(\tau, R, X)/V_{ss}(R, X) \geqslant e \tag{8}$$

is referred to as X_{BL}. For the results presented here, e was taken to be 0.01. The penetration distance obtained by applying the criterion of no overshoot in the mass flow rate during the one-dimensional process, as proposed by Joshi [14], is

$$X_J = \int_0^{R_\infty} U_{ss}(R, X) R\, dR \geqslant \int_0^{R_\infty} U(\tau, R) R\, dR. \tag{9}$$

Values of these penetration distances are compared later on.

3. SOLUTION

The governing boundary layer equations (1)–(3) subject to the boundary and initial conditions (4) are solved by a fully implicit finite difference marching technique. This technique is a modified form of the one described by Hornbeck [29] for flow through a circular pipe. While marching in the axial direction, the nonlinearity of the inertial terms and the interlinkage of momentum and energy equations are retained. Thus the finite difference form of equations (1)–(4) are solved iteratively by the Thomas Algorithm for tridiagonal equations [29] at any axial position. This iterative axial marching is repeated at each time step. Since the method is fully implicit, there is no constraint on the time step due to stability considerations.

3.1. *Computational details*

Variable grid sizes were used in the axial and radial directions. Figure 1(a) shows the steady-state values of the surface temperature $T_s(X)$ (solid line) and the maximum value of the axial velocity component U_{max} (dashed line) for $NX = 60$ and 120, where NX is the number of grids in the X-direction. A maximum difference of 2.6% is observed in U_{max} near the leading edge and only 0.6% near the downstream end. The corresponding differences in $T_s(X)$ are 1.1 and 0.2%. Thus, NX is taken to be 60 for all the results presented here. Grid size (ΔX) in the marching direction was taken as 0.2 near the upstream leading edge, and was increased to 2.0 far away from the leading edge. The adequate number of grid points in the radial direction, also determined in a similar manner, was found to increase with decreasing cylinder radius. The number of grids in the R-direction was 171 for a cylinder of $4 \leqslant R_0 \leqslant 50$ but it was required to increase it to 551 for $R_0 = 0.5$. Also, the smaller the value of R_0, the finer was the radial grid size near the surface of the cylinder in order to take care of increasing curvature

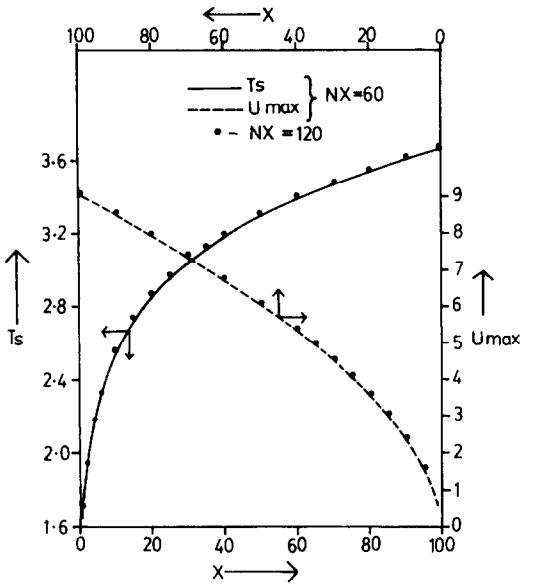

FIG. 1(a). Steady-state temperature and maximum value of axial velocity.

effects. The radial grid size near the cylinder for $R_0 = 4$ was 0.1. This was reduced to 0.0125 for $R_0 = 0.5$.

The step size in time, $\Delta\tau$, was steadily increased from a small initial value. Figure 1(b) shows the transient Nusselt number and dimensionless shear stress at $X = 100$ for two different $\Delta\tau$ ranges. Values of $\Delta\tau$ in the first range (solid lines) are four times those in the second range (solid circles). The two results are almost indistinguishable for $\tau \geqslant 4$, that is, for almost the entire duration of the transient. It may be pointed out that Ingham [30] could not get a $\Delta\tau$-independent heat transfer coefficient for the case of a flat plate when its temperature is suddenly increased from that of the surrounding fluid. In the present study, we did not observe such a phenomenon in any of the cases analyzed. Typical values of $\Delta\tau$ used in the study are $\Delta\tau = 0.1$ for $0 < \tau \leqslant 1$, $\Delta\tau = 1$ for $1 < \tau \leqslant 10$, $\Delta\tau = 5$ for $10 < \tau \leqslant 300$, $\Delta\tau = 20$ for $300 < \tau \leqslant 400$, $\Delta\tau = 50$ for $400 < \tau \leqslant 1000$, $\Delta\tau = 200$ for $1000 < \tau \leqslant 5000$, and $\Delta\tau = 1000$ for $\tau > 5000$.

To terminate the iteration of the linked finite difference form of equations (1)–(3) at any axial location X and time τ, the axial velocity distribution between two consecutive iterations satisfied the criterion

$$|1 - U^m(X, R, \tau)/U^{m+1}(X, R, \tau)| \leqslant \varepsilon \quad \text{for all } R \geqslant R_0$$

where m is the iteration index. The value of ε was taken to be 10^{-3} for the results presented here. The number of iterations was around 11 for X-locations away from the leading edge and was as high as 30 near the leading edge. Also, these numbers were found to increase with increasing cylinder radius. A relaxation factor of 0.6 was necessary for momentum and energy equations to converge.

3.2. *Accuracy*

In order to check our numerical procedure, we compared our steady-state finite difference solutions for isothermal cylinders with the local non-similar solutions of Minkowycz and Sparrow [24]. Figure 2 shows this comparison of boundary layer temperature for air with $Pr = 0.733$ and for two values of the stretched axial coordinate $\xi = 0.5$ and 2.0. There is an excellent match between the two solutions. Also, we compared our steady average heat transfer coefficient with the correlations proposed by Nagendra *et al.* [25]. Table 1 shows this comparison for $X = 100$ and $Pr = 0.72$. This value of X corresponds to a local Grashof number of 10^8. A maximum deviation of 10% is observed. Noting that the correlations of Nagendra *et al.* [25] were based on the experimental data for water and not for air ($Pr = 0.72$), and that the experimental data are from one source only, the agreement is quite satisfactory.

As already mentioned, the steady-state surface tem-

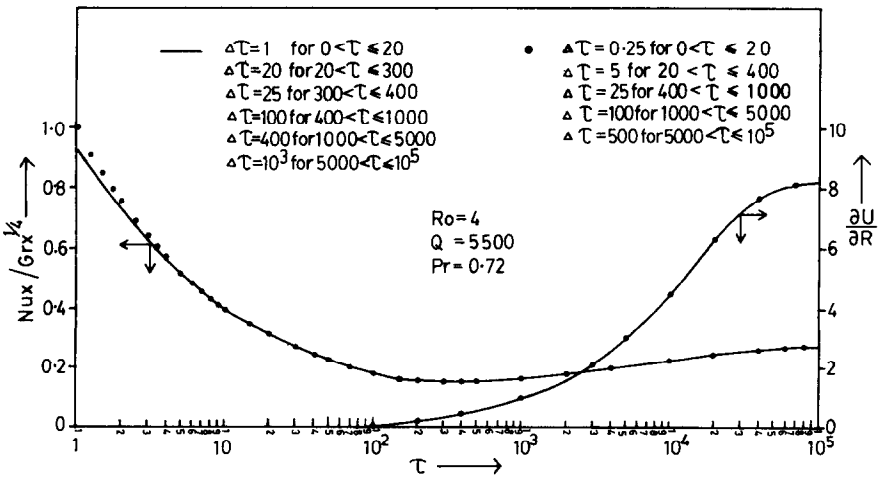

FIG. 1(b). Transient Nusselt number and shear stress at $X = 100$.

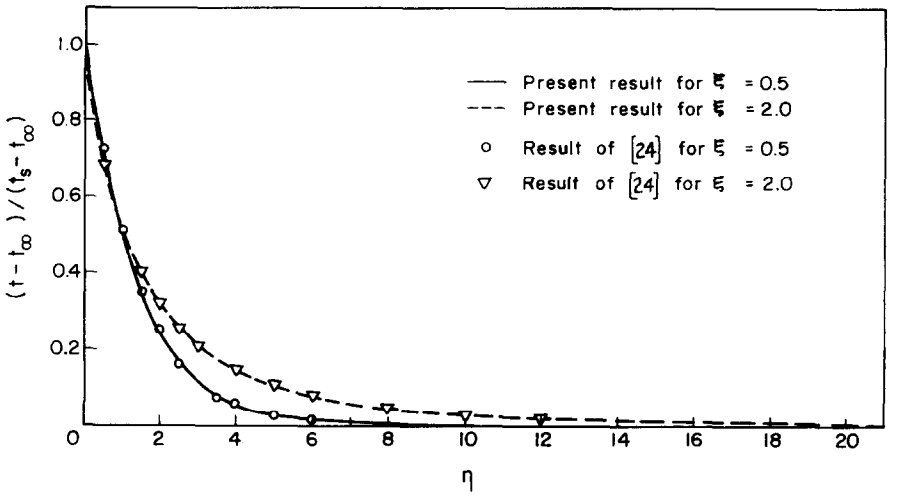

FIG. 2. Boundary layer temperature for isothermal cylinders.

Table 1. Comparison of average heat transfer coefficient

		$\overline{Nu}/Gr_L$		
R_0	$\eta_w(X_{end} = 100)$	Present	Nagendra *et al.* [25]	Deviation (%)
0.5	0.1443 (wire)	0.745	0.710	5
1.5	0.4328 (slender cylinder)	0.440	0.480	8
4.0	1.1542 (slender cylinder)	0.320	0.357	10

Table 2. Values of a and b in $T_s = bX^a$

		a		
R_0	$\eta_w(X_{end} = 100)$	Present	Nagendra *et al.* [25]	b (Present)
0.5	0.1443 (wire)	0.0875	0.04	0.9653
1.5	0.4328 (slender cylinder)	0.1288	0.138	1.4351
4.0	1.1542 (slender cylinder)	0.1631	0.138	1.7363
15.0	4.3281 (short cylinder)	0.1941	0.2	1.8922
50.0	14.427 (short cylinder)	0.2012	0.2	1.9574

perature of the cylinder is found to vary as $T_s = bX^a$, where the constants a and b vary with R_0. The values of a and b for various values of R_0 and the corresponding values of $\eta_w = R_0(5X)^{-1/5}$ at $X = 100$ are presented in Table 2. Also included in this table is the value of a from Nagendra *et al.* [25]. It is expected that the values of constant b and exponent a be continuous functions of R_0. However, only three discrete values are given in Nagendra *et al.* [25]. For two slender cylinders of radii $R_0 = 1.5$ and 4.0, the values of exponent a are 0.1288 and 0.1631, respectively. These values of a are on either side of the single value 0.138 given by Nagendra *et al.* [25]. For higher values of R_0 (short cylinders), the value of a approaches that for the flat plate, namely 0.2, in the present study as well as in Nagendra *et al.* [25]. It is found that the smaller the radius, the more uniform is the surface temperature of the cylinder.

For $R_0 = 4$, $Pr = 1$ and $Q = 0$, the transient velocity values and the penetration distance X_{GB} of the leading edge effect obtained from the solution of equations (5) and (6) at time $\tau = 16 \times 10^4$ are shown in

Table 3. Values of U and X_{GB} for $Pr = 1$, $Q = 0$ and $R_0 = 4$ at $\tau = 16 \times 10^4$

	$U/(2\pi R_0\tau)$			$X_{GB}/(2\pi R_0\tau^2)$		
r/r_0	Present	Goldstein and Briggs [8]	Percentage difference (%)	Present	Goldstein and Briggs [8]	Percentage difference (%)
2	1.2080	1.2088	0.07	0.6426	0.6393	0.51
5	2.7785	2.7781	0.01	1.4689	1.4602	0.60
15	4.4652	4.4646	0.01	2.2988	2.2845	0.63
25	4.9993	4.9991	0.004	2.4952	2.4791	0.65
30	5.1074	5.1074	0.00	2.5077	2.4911	0.67
35	5.1510	5.1513	0.006	2.4870	2.4700	0.69
40	5.1464	5.1469	0.01	2.4426	2.4255	0.71
70	4.5681	4.4698	0.04	1.9492	1.9332	0.83
150	2.1588	2.1606	0.08	0.6903	0.6818	1.24

Table 3. Here

$$X_{GB}(\tau, R) = \int_0^\tau U(\psi, R)\, d\psi.$$

Also presented in Table 3 are the closed form analytical solutions of Goldstein and Briggs [8] obtained through Laplace transforms. The present numerical values of U match very well with the analytical values; the maximum difference being only 0.08%. The values of penetration distance X_{GB} also match well with a maximum difference of 1.2%. The grid size in the radial direction for the numerical results in Table 3 was increased from 0.25 near the cylinder surface to 5.0 away from the cylinder. It may be pointed out that for the boundary layer solutions reported here for $R_0 = 4$, the corresponding values of ΔR are much smaller, being only 0.1 and 1.0, respectively.

4. RESULTS AND DISCUSSION

The steady-state profiles of the axial velocity component and temperature within the boundary layer are shown in Figs. 3(a) and (b) for $R_0 = 4$ and $Pr = 0.72$ at various axial positions from $X = 10$ to 100. This value of R_0 corresponds to $\eta_w = 1.1542$ (when $X_{end} = 100$) and falls under the category of slender cylinders [25]. For a cylinder of 4 mm radius in air, $R_0 = 4$ implies a surface heat flux of about 462 W m^{-2} and an internal energy generation rate of about 231 kW m^{-3}. The axial velocity and the boundary layer thickness increase in the flow direction as more and more fluid from the free stream entrains into the boundary layer. The peak in the axial velocity shifts outward as the flow develops axially due to increasing drag and decreasing entrainment velocity. The maximum value of the boundary layer velocity at $X = 100$ is 9.1, which corresponds to a physical value of about 0.19 m s^{-1} in air. The entrainment velocity was observed to be a maximum near the upstream end and decrease in the flow direction. The thermal boundary layer thickness and the surface temperature of the cylinder increase in the flow direction.

The transient radial velocity profile at $\tau = 150$ and the axial velocity profile at $\tau = 200$ are shown in Figs.

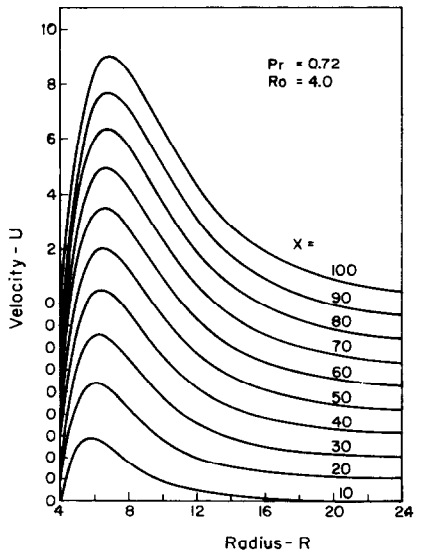

FIG. 3(a). Steady-state axial velocity profiles at various X locations.

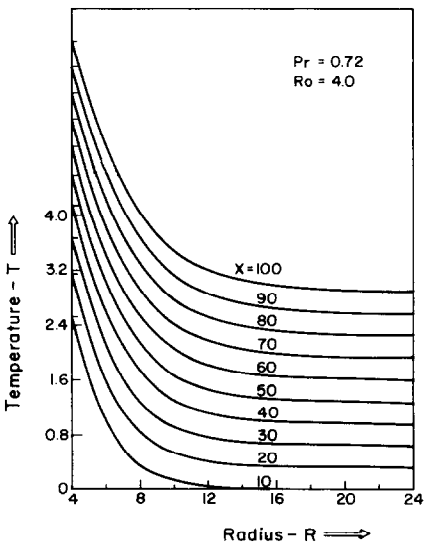

FIG. 3(b). Steady-state temperature profiles at various X locations.

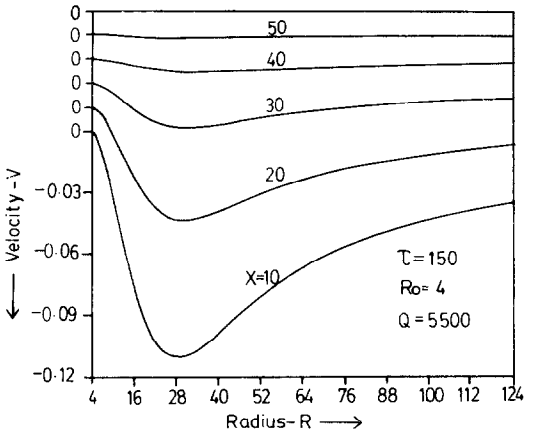

FIG. 4(a). Transient radial velocity profiles at various axial locations.

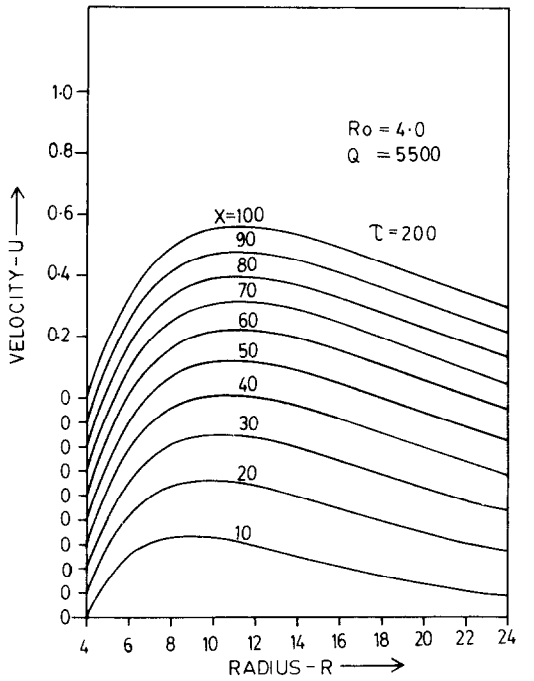

FIG. 4(b). Transient axial velocity profiles at various axial locations.

4(a) and (b), respectively, for $R_0 = 4$ and $Q = 5500$. This value of Q corresponds to a cylinder of stainless steel-316 in air at about 70°C. The penetration distance of the leading edge effect evaluated from the present boundary layer solution for various values of Q is shown in Fig. 5 (solid lines) for $R_0 = 4$. It may be noted that $Q = 4600$ and 3700 correspond to cylinder material of copper and tungsten, respectively. It is clear from Fig. 4(a) that the entrainment velocity is non-zero up to $X = 40$ and is zero for $X \geqslant 50$. This implies that the instantaneous location of the leading edge effect is between $X = 40$ and 50. From Fig. 5, we find that at $\tau = 150$ the leading edge effect is located at $X = 42$ for $Q = 5500$.

When $\tau = 200$, it is clear from Fig. 4(b) that the axial velocity profiles for $X \leqslant 80$ are different from each other while the velocity profiles for $X > 80$ are exactly the same as at $X = 80$. This implies that one-dimensional conduction governs the flow and associated fields for $X \geqslant 80$. Again from Fig. 5, the axial position of the leading edge effect at $\tau = 200$ is 78 for $Q = 5500$.

From Fig. 5, we find that the time required for the leading edge effect to reach $X = 100$ is 210 for $Q = 4600$. For $r_0 = 4$ mm and $R_0 = 4$, this corresponds to a physical time of about 10 s. It is also evident from Fig. 5 that the leading edge effect propagates faster as the thermal capacity decreases. This is due to the fact that the transient velocity associated with materials of smaller thermal capacity is higher since the heat flux on the cylinder is higher. Clearly, for the same energy generation rate, the transient heat flux is higher (as the absorption is less) for smaller thermal capacity.

Also shown in Fig. 5 are the penetration distances of the leading edge effect (i) from the solution of equation (7) (dashed lines), and (ii) by applying the criterion of no overshoot in the mass flow rate during the one-dimensional process [14] (chain lines). It is clear that equations (5)–(7) predict a slower rate of propagation of the leading edge effect than the actual value corresponding to the boundary layer solution for all the values of Q. It should be mentioned that exactly the same conclusion was drawn by earlier studies for a flat plate [14]. It is found that the time required for the leading edge effect to reach $X = 100$ based upon the solution of equation (7) is 21.1, 23.8 and 24% higher than the actual time based upon the boundary layer solution for $Q = 5500$, 4600 and 3700, respectively. For smaller values of X, however, these differences are larger. It is worth mentioning here that Mollendorf and Gebhart [9], and Mahajan and Gebhart [10] also observed the actual propagation rate to be 20% faster than that predicted by Goldstein and Briggs [8] for a flat plate. Also, the prediction of Goldstein and Briggs [8] is not much different [14] from that of equation (7). For a flat plate, Joshi [14] found that the criterion of no overshoot in the mass flow rate during the one-dimensional process predicts a faster rate of propagation of the leading edge effect than that based upon equation (7). For the case of a cylinder, however, the reverse is true for all values of Q, as is evident from the results in Fig. 5.

The transient local Nusselt number is shown in Figs. 6(a) and (b) for $Q = 3700$ and 5500, respectively, when $R_0 = 4$. It can be seen that the Nusselt number profile at any instant is made up of two parts, namely, (i) the part near the upstream end (small X-values), and (ii) the part near the downstream end (large X-values) where the Nusselt number is independent of X. While part (i) corresponds to the region of the cylinder surface through which the leading edge effect has already passed, part (ii) corresponds to the region where this effect has yet to reach and the one-dimen-

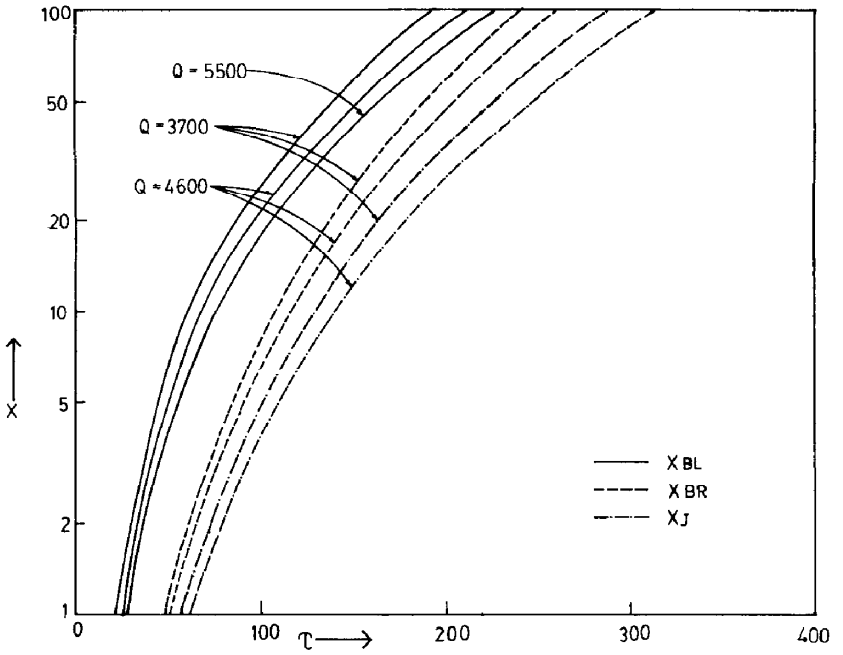

FIG. 5. Penetration distance of leading edge effect for $R_0 = 4$.

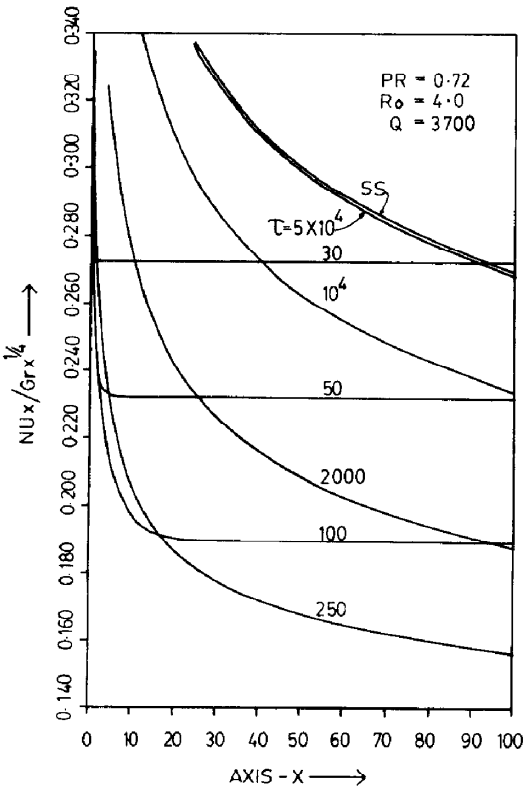

FIG. 6(a). Local Nusselt number for $R_0 = 4$ and $Q = 3700$.

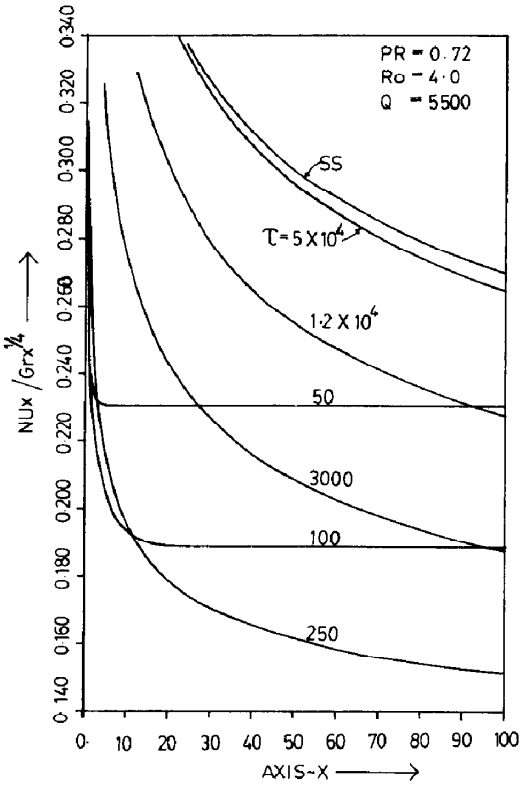

FIG. 6(b). Local Nusselt number for $R_0 = 4$ and $Q = 5500$.

sional conduction regime prevails as is evident from the constant value of the Nusselt number. The patching point of the two parts denotes the instantaneous location of the leading edge effect. For example, for $Q = 3700$ at $\tau = 100$, this point lies around $X = 25$ and the actual value of the penetration distance at this instant from Fig. 5 is 26. Moreover, it may be noted that this point moves downstream with time.

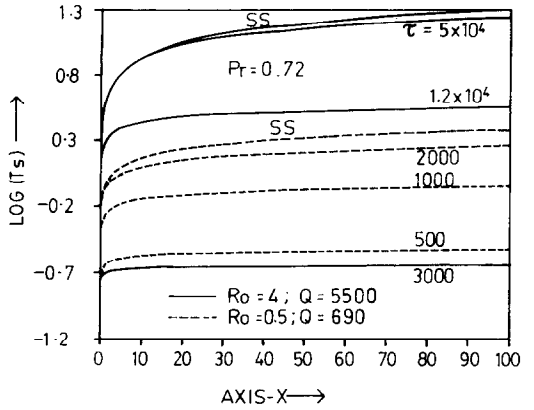

FIG. 7. Transient surface temperature at various instants.

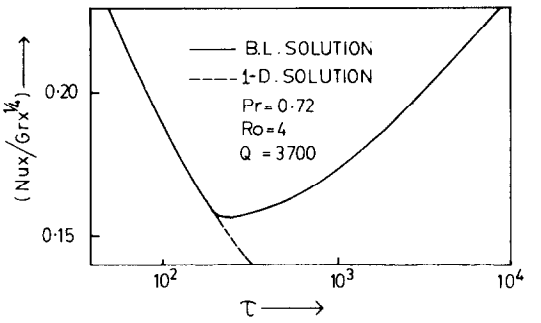

FIG. 8. Comparison of boundary layer and one-dimensional solutions.

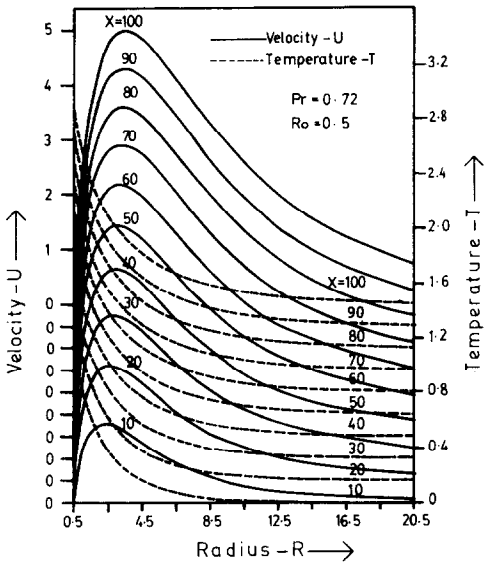

FIG. 9. Steady-state axial velocity and temperature profiles for $R_0 = 0.5$.

It is also evident from Fig. 6 that the Nusselt number at any location passes through a minimum before reaching the steady-state value. A closer look at Fig. 6 reveals that the heat transfer coefficient at any instant and at any location is higher for smaller values of Q, owing to higher transient heat flux. Similar results were also obtained for other values of Q. The physical value of the steady-state heat transfer coefficient at $X = 100$ is about 8.1 W m^{-2} K^{-1} for a cylinder of 4 mm radius in air.

The transient surface temperature evolution is shown in Fig. 7 for $R_0 = 4$ and $Q = 5500$ (solid lines). For this case the time required to reach steady state is around $\tau = 10^5$ which corresponds to a physical time of about 4800 s in air for a cylinder of 4 mm radius. For the same R_0 and for other values of Q, the temperature evolution was found to be similar but at a slightly faster rate. We may also mention that no overshoot either in the boundary layer temperature or velocity was found in the entire parameter range reported here. However, an overshoot in the temperature as well as the velocity profiles is observed when $Q = 0$ or small. The absence of an overshoot for the large values of Q is due to the fact that the ratio of the heat capacity of the solid to that of air is very high. For example, for stainless steel-316 and air, this ratio is about 3000. Thus, for large values of Q, the temperature rise of the cylinder is too slow for the thermal capacity of the boundary layer fluid and the time for boundary layer development to produce any temperature or velocity overshoot.

Figure 8 shows the transient evolution of the Nusselt number at $X = 100$ from the boundary layer (solid line) and the one-dimensional (dashed line) solutions for $R_0 = 4$ and $Q = 3700$. The one-dimensional solution departs from the boundary layer solution at $\tau \approx 194$. From Fig. 5, we find that the leading edge effect for this case arrives at $X = 100$ when $\tau = 194$. This is an indirect validation for the value of $e = 0.01$ used in equation (8). The minimum value of the Nusselt number occurs, however, at $\tau = 230$. Table 4 shows the minimum values of the Nusselt number at $X = 100$, the time when this minimum occurs, and the time when the leading edge effect reaches $X = 100$ for $R_0 = 4$ and various values of Q. Clearly, the minimum Nusselt number occurs well after the arrival of the leading edge effect. Also, the higher the heat capacity Q, the lower is the minimum Nusselt number.

Results for two more values of R_0, namely, 0.5 and 1.5, were also computed. For a given fluid, different values of R_0 correspond to a different radius of the cylinder and/or a different value of the heat flux q''. The steady-state profiles of axial velocity component and temperature within the boundary layer for $R_0 = 0.5$ are shown in Fig. 9. This value of R_0 cor-

Table 4. Local Nusselt number for $R_0 = 4$ and $Pr = 0.72$

Q	$(Nu_x/Gr_x^{1/4})_{min}$ at $X = 100$	τ when Nu_{min} occurs	τ when L.E.E. crosses $X = 100$
5500	0.1505	260	228
4600	0.1528	245	210
3700	0.1558	230	194

responds to a value of $\eta_w = 0.1443$ (when $X_{end} = 100$) and falls under the category of wires [25]. While the boundary layer thickness increases with a reduction in R_0, the boundary layer velocity decreases as the cylinder gets thinner. A reduction in the cylinder radius leads to a reduction in the surface area per unit length and hence in the total energy generation rate. These in effect reduce the boundary layer temperature and buoyancy force leading to a reduction in the velocity within the boundary layer. The steady-state surface temperature for $R_0 = 0.5$ (dashed line) is shown in Fig. 7. From this figure, it is clear that the thinner the cylinder, the more uniform is the surface temperature. The reason for this can be explained as follows.

The thinner the cylinder, the thicker the boundary layer and hence the greater the quantity of fluid exchanging heat. Also, the thinner the cylinder, the smaller the total energy generated. Since the total energy to be convected away from the cylinder is smaller while the fluid available for heat exchange is greater, the surface temperature tends to be more uniform.

Also shown in Fig. 7 is the transient evolution of the surface temperature for $R_0 = 0.5$ and $Q = 690$. This value of Q corresponds to a cylinder of stainless steel-316 in air at about 70°C. This is also the case for $Q = 2060$ when $R_0 = 1.5$. The surface temperature evolution for $R_0 = 1.5$ and $Q = 2060$ is also similar except that its evolution rate lies between the two cases reported in Fig. 7. The penetration distance of the leading edge effect from the boundary layer and one-dimensional analyses are shown in Fig. 10 for $R_0 = 0.5$ and $Q = 690$. The dimensionless time required for the leading edge effect to reach $X = 100$ is 125. This corresponds to a physical time of about 6 s for a cylinder of 1 mm diameter in air. Similarly, from the results for $R_0 = 1.5$ and $Q = 2060$, the physical time required for the leading edge effect to reach $X = 100$ is found to be 8.2 s for a cylinder of 3 mm diameter in air. Comparing Figs. 5 and 10, we find that for the same heat flux value and the same cylinder material, the leading edge effect propagates faster for a thinner cylinder. Despite the fact that the axial velocity component associated with a thinner cylinder is smaller, the transient evolution of the boundary layer velocity is faster than that for thicker cylinders.

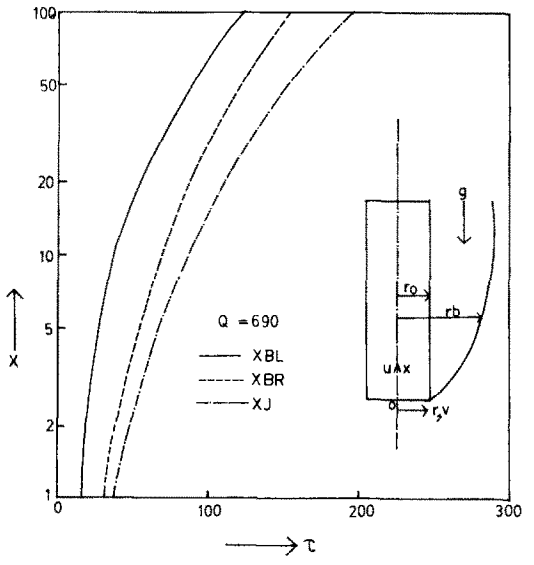

FIG. 10. Penetration distance of leading edge effect for $R_0 = 0.5$.

Similar to the observation made for the results in Fig. 5, the propagation rates of the leading edge effect estimated from the one-dimensional analyses are slower than the real one for $R_0 = 0.5$. The time required for the leading edge effect to reach $X = 100$ based upon equation (7) is 24% larger than the real one. Moreover, the criterion of no overshoot in the mass flow rate during the one-dimensional process also predicts a slower propagation rate than that from equation (7), which is contrary to the observation made for a flat plate by Joshi [14]. Similar conclusions also hold for $R_0 = 1.5$.

The evolution of the transient Nusselt number for $R_0 = 1.5$ and 0.5 is similar to that for $R_0 = 4$ shown in Fig. 6, except for a faster rate of evolution and a higher Nusselt number as R_0 decreases. For example, for $R_0 = 1.5$ and 0.5, the physical values of heat transfer coefficient at $X = 100$ are 11.4 and 20.4 W m^{-2} K^{-1}, respectively, for cylinders of radii 1.5 and 0.5 mm.

The transient values of average Nusselt number, $\overline{Nu}$, averaged over the length of the cylinder, are shown in Figs. 11(a) and (b) for various values of Q and R_0. Similar to the local Nusselt number, $\overline{Nu}$ passes through a minimum for all values of R_0 and Q. For the same heat flux and cylinder material, the thinner the cylinder, the earlier this minimum appears. Also, for the same radius r_0 and heat flux, the smaller the heat capacity of the material, the earlier this minimum appears. For $R_0 = 4$ and $Q = 5500$, $\overline{Nu}$ reaches a minimum value of about 53% of the steady-state value. However, as the heat capacity or cylinder radius decreases, this minimum value increases.

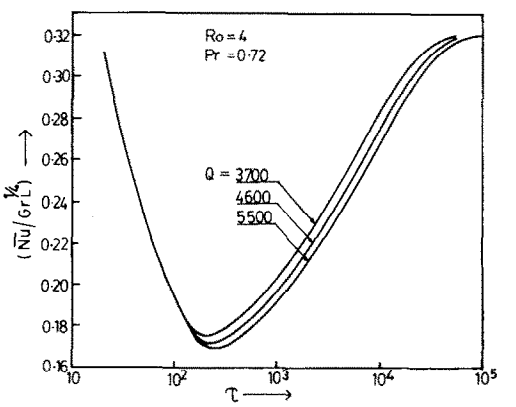

FIG. 11(a). Transient average Nusselt number for $R_0 = 4$.

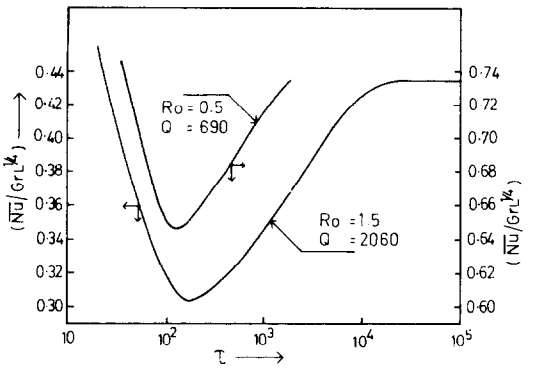

FIG. 11(b). Transient average Nusselt number for $R_0 = 0.5$ and 1.5.

Figure 12 shows the transient extension of the boundary layer, R_b, at the downstream location $X = 100$ for various values of R_0 and Q. The edge of the boundary layer was assumed to be the location where the axial velocity component U reached a value of 0.001. Clearly, the thinner the cylinder, the thicker the steady-state boundary layer. For example, for a cylinder of 4 mm radius in air, the steady-state boundary layer thickness is 93 mm, while for a 0.5 mm radius cylinder, it is 131 mm for all cylinder materials and heat fluxes investigated.

The transient boundary layer thickness exceeds its steady-state value for all the values of R_0 and Q. For example, for $R_0 = 4$ and $Q = 5500$, the transient boundary layer thickness exceeds the steady-state value by about 24%. This value decreases as either the heat capacity or the radius decreases. Another observation is that this peak appears well after the passage of the leading edge effect.

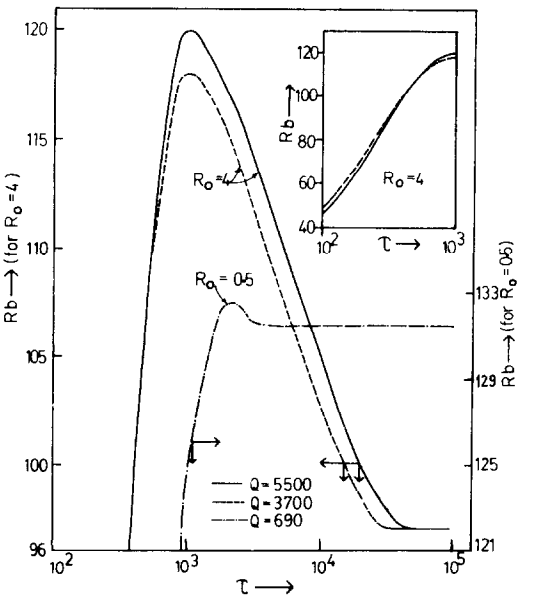

FIG. 12. Transient boundary layer thickness.

5. CONCLUSIONS

The transient boundary layer equations for free convection adjacent to a heat generating vertical cylinder have been solved numerically. The following conclusions are drawn:

(a) The rate of propagation of the leading edge effect for cylinders, predicted by the one-dimensional conduction equations and equation (7), is found to be slower than the actual value predicted by the boundary layer equations.

(b) The criterion of no overshoot in the mass flow rate during the one-dimensional process predicts a slower rate of propagation of the leading edge effect than that from equation (7) for the case of a cylinder, while the reverse is true for a flat plate [14].

(c) The rate of propagation of the leading edge effect decreases as the radius and thermal capacity of the cylinder increase, and as the heat flux decreases.

(d) The local Nusselt number passes through a minimum during the transient for all values of the cylinder radius, thermal capacity, and heat flux. Similarly, the average Nusselt number also passes through a minimum. The latter reaches a minimum value as low as 53% of its steady-state value for the largest R_0 and Q considered. The minimum value increases as either the heat capacity or the cylinder radius decreases, and is found to occur well after the leading edge effect crosses that axial position.

(e) During the transient, the boundary layer thickness exceeds its steady-state value. This value is about 1.24 times the steady-state value for the largest R_0 considered, and decreases with either the heat capacity or the cylinder radius. Moreover, the peak value appears long after the passage of the leading edge effect.

(f) The steady surface temperature distribution of the cylinder for any R_0 is found to vary as $T_s = bX^a$, where the values of a and b are presented for R_0 varying from 0.5 to 50.

Acknowledgements—The computing facilities at the Indira Gandhi Centre for Atomic Research and at the University of Pittsburgh are gratefully acknowledged. The authors would also like to acknowledge the referees for their useful and stimulating comments.

REFERENCES

1. C. R. Illingworth, Unsteady laminar flow of gas near an infinite plate, *Proc. Camb. Phil. Soc.* **46**(4), 603–613 (1950).
2. J. A. Schetz and R. Eichhorn, Unsteady natural convection in the vicinity of a doubly infinite vertical plate, *J. Heat Transfer* **84**, 334–338 (1962).
3. E. R. Menold and K. Yang, Asymptotic solutions for laminar free convection on a vertical plate, *J. Appl. Mech.* **84**, 124–126 (1962).
4. R. Siegel, Transient free convection from a vertical flat plate, *J. Heat Transfer* **80**, 347–359 (1958).
5. R. J. Goldstein and E. R. G. Eckert, The steady and transient free convection boundary layer on a uniformly

heated vertical plate, *Int. J. Heat Mass Transfer* **1**, 208–218 (1960).
6. B. Gebhart, Transient natural convection from vertical elements, *J. Heat Transfer* **83**, 61–70 (1961).
7. B. Gebhart and D. E. Adams, Measurements of transient natural convection in flat vertical surfaces, *J. Heat Transfer* **84**, 1–4 (1962).
8. R. J. Goldstein and D. G. Briggs, Transient free convection about vertical plates and circular cylinders, *J. Heat Transfer* **86**, 490–500 (1964).
9. J. C. Mollendorf and B. Gebhart, An experimental study of vigorous transient natural convection, *J. Heat Transfer* **92**, 628–634 (1970).
10. R. L. Mahajan and B. Gebhart, Leading edge effects in transient natural convection flow adjacent to a vertical surface, *J. Heat Transfer* **100**, 731–733 (1978).
11. K. T. Yang, Remarks on transient laminar free convection along a vertical plate, *Int. J. Heat Mass Transfer* **9**, 511–513 (1966).
12. K. Nanbu, Limit of pure conduction for unsteady free convection on a vertical plate, *Int. J. Heat Mass Transfer* **14**, 1531–1534 (1971).
13. S. N. Brown and N. Riley, Flow past a suddenly heated vertical plate, *J. Fluid Mech.* **59**, 225–237 (1973).
14. Y. Joshi, On the termination of one-dimensional transport in transient buoyancy induced flow adjacent to a vertical surface, *Int. J. Heat Mass Transfer* **30**, 1766–1769 (1987).
15. J. D. Hellums and S. W. Churchill, Transient and steady state, free and natural convection, numerical solutions: Part I. The isothermal vertical plate, *A.I.Ch.E. Jl* **8**, 690–692 (1962).
16. B. Sammakia, B. Gebhart and Z. H. Qureshi, Measurements and calculations of transient natural convection in air, *Int. J. Heat Mass Transfer* **23**, 571–576 (1980).
17. B. Sammakia, B. Gebhart and Z. H. Qureshi, Measurements and calculations of transient natural convection in water, *J. Heat Transfer* **104**, 644–648 (1982).
18. V. P. Carey, Analysis of transient natural convection flow at high Prandtl number using a matched asymptotic expansion technique, *Int. J. Heat Mass Transfer* **26**, 911–919 (1983).
19. V. P. Carey, Surface thermal capacity effects in transient natural convection flows at high Prandtl number, *Int. J. Heat Mass Transfer* **27**, 419–431 (1984).
20. Y. Joshi and B. Gebhart, Vertical transient natural convection flows in cold water, *Int. J. Heat Mass Transfer* **27**, 1573–1582 (1984).
21. Y. Joshi and B. Gebhart, Transient response of a steady vertical flow subject to a change in surface heating rate, *Int. J. Heat Mass Transfer* **31**, 743–757 (1988).
22. M. Y. Gokhle, Finite difference analysis of the transient free convection on an isothermal plate with temperature gradient dependent heat source, *Int. J. Heat Technol.* **6**, 61–74 (1988).
23. R. P. Dring and B. Gebhart, Transient natural convection from thin vertical cylinders, *J. Heat Transfer* **88**, 246–247 (1966).
24. W. J. Minkowycz and E. M. Sparrow, Local nonsimilar solutions for natural convection on vertical cylinders, *J. Heat Transfer* **96**, 178–183 (1974).
25. H. R. Nagendra, M. A. Tirunarayanan and A. Ramachandran, Laminar free convection from vertical cylinders with uniform heat flux, *J. Heat Transfer* **92**, 191–194 (1970).
26. T. S. Chen and C. F. Yuh, Combined heat and mass transfer in natural convection along vertical cylinder, *Int. J. Heat Mass Transfer* **23**, 451–461 (1980).
27. J. L. S. Chen, Natural convection from needles with variable wall heat flux, *J. Heat Transfer* **105**, 403–406 (1983).
28. H. R. Lee, T. S. Chen and B. F. Armaly, Natural convection along slender vertical cylinders with variable surface temperature, *J. Heat Transfer* **110**, 103–108 (1988).
29. R. W. Hornbeck, Numerical marching techniques for fluid flow with heat transfer, NASA SP-297, Washington, DC (1973).
30. D. B. Ingham, Numerical results for flow past a suddenly heated vertical plate, *Physics Fluids* **21**, 1891–1895 (1978).

CONVECTION NATURELLE VARIABLE SUR UN CYLINDRE VERTICAL CHAUFFE

Résumé—On présente une solution numérique pour la convection naturelle variable sur des cylindres verticaux chauffés, de capacités thermiques et de rayons différents. Une technique de différences finies entièrement implicite est utilisée pour résoudre le système d'équations non linéaire. On porte une considération particulière sur l'effet de la vitesse de propagation du bord d'attaque. On trouve que cette vitesse, prédite par la solution de conduction monodimensionnelle, est plus lente que celle résultant de la solution de couche limite. Elle augmente quand le rayon et la capacité thermique diminuent et quand le flux thermique à la surface augmente. L'épaisseur de couche limite variable excède sa valeur stationnaire tandis que le coefficient moyen de transfert atteint un minimum allant jusqu'à 53% de sa valeur stationnaire pour la plus grande valeur étudiée du nombre de Grashof. Un accord excellent est obtenu avec les données expérimentales du régime stationnaire ainsi qu'avec les résultats théoriques connus en monodimensionnel.

INSTATIONÄRE NATÜRLICHE KONVEKTION OBERHALB EINER VERTIKALEN ZYLINDRISCHEN WÄRMEQUELLE

Zusammenfassung—Für die instationäre natürliche Konvektion oberhalb eines vertikalen wärmeerzeugenden Zylinders mit unterschiedlichen Wärmekapazitäten und Radien werden numerische Lösungen angegeben. Für die Lösung des nichtlinearen Gleichungssystems wird ein implizites Finite-Differenzen-Verfahren verwendet. Der Ausbreitungsgeschwindigkeit des Anströmeffektes wird besondere Aufmerksamkeit gewidmet. Es zeigt sich, daß die durch eine eindimensionale Wärmeleitungsgleichung vorhergesagte Geschwindigkeit geringer ist als die durch die Grenzschichttheorie vorhergesagte. Außerdem wächst sie mit abnehmenden Werten von Radius und Wärmekapazität des Zylinders, aber auch durch Erhöhung der Wärmestromdichte. Die Dicke der instationären Grenzschicht ist größer als im stationären Fall, wogegen der instationäre mittlere Wärmeübergangskoeffizient ein Minimum erreicht, welches bei der größten verwendeten Grashof-Zahl 53% des stationären Wertes beträgt. Die Übereinstimmung mit früher gemessenen Werten für den stationären Fall und auch mit theoretischen Ergebnissen für den eindimensionalen Fall sind ausgezeichnet.

НЕСТАЦИОНАРНАЯ ЕСТЕСТВЕННАЯ КОНВЕКЦИЯ У ТЕПЛОВЫДЕЛЯЮЩЕГО ВЕРТИКАЛЬНОГО ЦИЛИНДРА

Аннотация—Представлено численное решение задачи нестационарной естественной конвекции у тепловыделяющих вертикальных цилиндров с различными радиусами и температурами. Нелинейная система уравнений решается неявным методом конечных разностей. Особое внимание обращается на интенсивность распространения эффеста передней кромки. Найдено, что значение интенсивности, полученное решением одномерного уравнения теплопроводности, меньше значения, определяемого из решения пограничного слоя. Кроме того, интенсивность растет с уменьшением радиуса и теплоемкости цилиндра и с увеличением теплового потока на поверхности. Иайдено, что толщина нестационарного пограничного слоя превышает стационарное значение, а значение нестационарного усредненного коэффициента теплопереноса достигает минимума, составляющего 53% стационарного значения для максимального модифицированного числа Грасгофа. Получено хорошее согласие с предыдущими экспериментальными стационарными данными, а также с одномерными теоретическими результатами.